

## AEGIS: NEW EVIDENCE LINKING ACTIVE GALACTIC NUCLEI TO THE QUENCHING OF STAR FORMATION

KEVIN BUNDY,<sup>1</sup> ANTONIS GEORGAKAKIS,<sup>2,3</sup> KIRPAL NANDRA,<sup>2</sup> RICHARD S. ELLIS,<sup>4</sup> CHRISTOPHER J. CONSELICE,<sup>4,5</sup>  
ELISE LAIRD,<sup>2</sup> ALISON COIL,<sup>6,7</sup> MICHAEL C. COOPER,<sup>6,8</sup> SANDRA M. FABER,<sup>9</sup> JEFF A. NEWMAN,<sup>10</sup>  
CHRISTY M. PIERCE,<sup>11</sup> JOEL R. PRIMACK,<sup>9</sup> AND RENBIN YAN<sup>12</sup>

Received 2007 October 10; accepted 2008 March 26

### ABSTRACT

Using *Chandra* X-ray observations in the All-Wavelength Extended Groth Strip International Survey (AEGIS) we identify 241 X-ray-selected active galactic nuclei (AGNs;  $L_{2-10} > 10^{42}$  ergs s<sup>-1</sup>) and study the properties of their host galaxies in the range  $0.4 < z < 1.4$ . By making use of infrared photometry from the Palomar Observatory and *BRI* imaging from the Canada-France-Hawaii Telescope, we estimate AGN host galaxy stellar masses and show that both stellar mass and photometric redshift estimates (where necessary) are robust to the possible contamination from AGNs in our X-ray-selected sample. Accounting for the photometric and X-ray sensitivity limits of the survey, we construct the stellar mass function of X-ray-selected AGN host galaxies and find that their abundance decreases by a factor of  $\sim 2$  since  $z \sim 1$  but remains roughly flat as a function of stellar mass. We compare the abundance of AGN hosts to the rate of star formation quenching observed in the total galaxy population. If the timescale for X-ray-detectable AGN activity is roughly 0.5–1 Gyr, as suggested by black hole demographics and recent simulations, then we deduce that the inferred AGN “trigger” rate matches the star formation quenching rate, suggesting a link between these phenomena. However, given the large range of nuclear accretion rates we infer for the most massive and red hosts, X-ray-selected AGNs may not be *directly* responsible for quenching star formation.

*Subject headings:* cosmology: observations — galaxies: evolution — galaxies: formation

*Online material:* color figures

### 1. INTRODUCTION

Recent observations of the galaxy population and its evolution since  $z \approx 2$  reveal a pattern in which the most massive galaxies appear to shut down star formation activity at early times, with increasingly less massive galaxies following later (e.g., Juneau et al. 2005; Treu et al. 2005; Bundy et al. 2006; Borch et al. 2006; Cimatti et al. 2006). This pattern of “quenching” in the star formation history of galaxies, thought to be largely responsible for the growing abundance of galaxies on the red sequence (e.g., Faber et al. 2007), is commonly referred to as “downsizing” (Cowie et al. 1996).

Given that the dark matter halos of galaxies are expected to assemble hierarchically in the  $\Lambda$ CDM paradigm, understanding the physical mechanisms responsible for downsizing remains an important challenge. We seek a process capable of quenching

star formation, driving galaxies onto the red sequence, and preventing further star formation. Work with the DEEP2 Galaxy Redshift Survey (Davis et al. 2003) has shown that such a process must operate over a range of environmental densities (Bundy et al. 2006; Cooper et al. 2007; Gerke et al. 2007), suggesting an internal component to quenching that acts in addition to the suppression of star formation expected in high-density environments. Meanwhile, theoretical work has focused on one such internal process, namely, the potential role played by active galactic nucleus (AGN) feedback (Silk & Rees 1998), as a way of both explosively initiating the quenching event (Granato et al. 2004; Scannapieco et al. 2005; Hopkins et al. 2005a) and preventing hot gas in already passive galaxies from cooling to form stars (Croton et al. 2006; Bower et al. 2006; Cattaneo et al. 2006; de Lucia & Blaizot 2007).

These scenarios remain largely untested because observational evidence has been difficult to obtain. One of the most promising ways forward is to examine the properties of AGN host galaxies and search for signatures of this feedback. Such observations are challenging, however, because no selection method finds all the galaxies that host active nuclei (Mushotzky 2004), and brighter AGNs (quasars) can easily outshine their hosts. With such difficulties in mind, previous studies suggest that most lower luminosity AGNs tend to be found in massive, mostly spheroidal galaxies (Dunlop et al. 2003; Kauffmann et al. 2003; Grogin et al. 2005; Pierce et al. 2007; Alonso-Herrero et al. 2008; Silverman et al. 2008), although some “transition” sources exhibit disturbed morphologies (e.g., Canalizo & Stockton 2001; Hutchings et al. 2006; Conselice et al. 2007). AGNs detected through emission-line diagnostics and X-rays appear to prefer host galaxies on the red sequence and “green valley” (Nandra et al. 2007; Martin et al. 2008; Salim et al. 2008).

Further progress on testing the link between AGN activity and the downsizing of star formation requires that we understand the stellar mass distribution and redshift evolution of AGN hosts as

<sup>1</sup> Reinhardt Fellow, Department of Astronomy and Astrophysics, University of Toronto, 50 St. George Street, Room 101, Toronto, ON M5S 3H4, Canada.

<sup>2</sup> Astrophysics Group, Blackett Laboratory, Imperial College, London SW7 2AZ, UK.

<sup>3</sup> Marie Curie Fellow.

<sup>4</sup> California Institute of Technology, 1201 East California Boulevard, MS 105-24, Pasadena, CA 91125.

<sup>5</sup> School of Physics and Astronomy, University of Nottingham, Nottingham NG7 2RD, UK.

<sup>6</sup> Steward Observatory, University of Arizona, 933 North Cherry Avenue, Tucson, AZ 85721.

<sup>7</sup> Hubble Fellow.

<sup>8</sup> Spitzer Fellow.

<sup>9</sup> University of California Observatories/Lick Observatory, University of California, Santa Cruz, CA 95064.

<sup>10</sup> Department of Physics and Astronomy, University of Pittsburgh, Pittsburgh, PA 15260.

<sup>11</sup> Department of Physics, University of California, Santa Cruz, 1156 High Street, Santa Cruz, CA 95064.

<sup>12</sup> Department of Astronomy, University of California, Berkeley, MC 3411, Berkeley, CA 94720.

compared to evolutionary patterns in the general galaxy population (e.g., Alonso-Herrero et al. 2008). In this paper we use deep *Chandra* observations to identify AGN hosts in the AEGIS field (Davis et al. 2007) where spectroscopic and photometric redshifts (photo-*z*s), as well as infrared photometry, provide reliable stellar mass estimates out to  $z = 1.4$ . We then compute the AGN host stellar mass function (MF) and use it to estimate the rate at which AGN activity is triggered in the galaxy population. We show that this mass-dependent rate is consistent with the rate of star formation quenching of all galaxies at the same epochs at which the AGN activity is observed.

The structure of the paper is as follows. We describe the multi-wavelength observations and properties of the sample in §§ 2 and 3. The way in which stellar masses and rest-frame colors are determined is given in § 4, while our methods for constructing MFs and the resulting AGN host MF are discussed in § 5. In § 6 we present evidence for a link between AGN activity and quenching in the context of estimates of the X-ray AGN timescale and explore whether feedback from X-ray-selected AGNs causes quenching. We summarize in § 7. Where necessary, we assume a standard cosmological model with  $\Omega_M = 0.3$ ,  $\Omega_\Lambda = 0.7$ ,  $H_0 = 70 h_{70} \text{ km s}^{-1} \text{ Mpc}^{-1}$ .

## 2. OBSERVATIONS

In this section we discuss the various observations we use to investigate the link between AGNs and galaxy evolution. We begin by summarizing the DEEP2 Galaxy Redshift Survey (Davis et al. 2003) and a follow-up infrared imaging campaign conducted at Palomar Observatory. One of the four fields in this survey, the Extended Groth Strip (EGS), was imaged with *Chandra* as part of the AEGIS program, providing the sample of AGN host galaxies that we use here. We compare the evolution of this AGN host sample to trends observed in galaxies drawn from the full DEEP2/Palomar survey. As discussed in Bundy et al. (2006), this sample provides robust stellar mass estimates that can be used to investigate mass-dependent evolution out to  $z = 1.4$ .

### 2.1. The DEEP2/Palomar Survey

We provide a brief summary of the DEEP2 Galaxy Redshift Survey and the near-infrared (near-IR) follow-up imaging conducted at Palomar Observatory. The data sets involved were used by Bundy et al. (2006) to explore the nature of star formation downsizing since  $z \approx 1.2$ , and further details are provided there. Now complete, the DEEP2 Galaxy Redshift Survey (Davis et al. 2003) used DEIMOS on the Keck II telescope to obtain spectroscopic redshifts for  $\sim 40,000$  galaxies with  $z \lesssim 1.5$ . The survey was magnitude-limited at  $R_{AB} \leq 24.1$  and covered more than  $3 \text{ deg}^2$  over four fields, one of which is the AEGIS field and is described further below.

Redshift targets were selected using *BRI* photometry from the Canada-France-Hawaii Telescope (CFHT) with the  $12\text{K} \times 8\text{K}$  mosaic camera (Cuillandre et al. 2001). As described in Coil et al. (2004), the photometry reached  $R_{AB} \sim 25.5$  and was also used for estimating photo-*z*s and rest-frame ( $U - B$ ) colors, as discussed below. In the three non-AEGIS fields, target selection in DEEP2 was carried out using observed colors to exclude sources with  $z < 0.7$ . These selection criteria successfully recovered 97% of the  $R_{AB} \leq 24.1$  population at  $z > 0.75$  with only  $\sim 10\%$  contamination from lower redshift galaxies (Davis et al. 2005). More details on the observing strategy and characteristics of the DEEP2 sample are provided in Coil et al. (2004), Willmer et al. (2006), Davis et al. (2005, 2007), Faber et al. (2007), and J. A. Newman et al. (in preparation).

Follow-up imaging of the DEEP2 survey in the *J* and  $K_s$  bands was carried out using the Wide Field Infrared Camera (Wilson et al.

2003) on the 5 m Hale Telescope at Palomar Observatory. These observations are discussed in detail in Bundy et al. (2006). Excluding the AEGIS field, which was the highest priority,  $0.9 \text{ deg}^2$  of DEEP2 were imaged primarily in the  $K_s$  band with exposure times varying from 2 to 8 hr, depending on the conditions, and the final typical 80% completeness depth of  $K_{AB} = 21.5$ .

We used SExtractor (Bertin & Arnouts 1996) to detect and measure  $K_s$ -band sources and cross-referenced them with the CFHT optical and DEEP2 redshift catalogs to construct the *K*-selected sample that forms the basis of our analysis. For total magnitudes used to estimate stellar masses, we took the MAG\_AUTO output from SExtractor and did not correct this Kron-like magnitude for missing light. We estimated the uncertainty on these magnitudes by inserting fake sources at various magnitudes and using SExtractor to recover them. Based on the locations of *K*-selected sources, we measured aperture photometry in the *BRI* data using  $2''$  diameter apertures, which we found exhibited the least scatter. These colors are used in fitting the galaxy spectral energy distributions (SEDs) needed for both photo-*z*s and stellar mass estimates.

### 2.2. The AEGIS Field

Covering the  $0.5 \text{ deg}^2$  EGS ( $\alpha = 14^{\text{h}} 17^{\text{m}}$ ,  $\delta = +52^\circ 30'$ ), the All-Wavelength Extended Groth Strip International Survey (AEGIS; Davis et al. 2007) accounts for one of the four fields where DEEP2 redshifts and Palomar near-IR imaging were obtained, although there are slight differences with respect to the other DEEP2 fields (above) that we describe here. This field is also special because many other observatories, including the *Hubble Space Telescope* and *Spitzer Space Telescope*, have conducted observations there. Of key importance for this work are the deep X-ray data from the Advanced CCD Imaging Spectrometer (ACIS) on *Chandra*.

The *Chandra* data are described in Georgakakis et al. (2006, 2007), and the X-ray data analysis is presented in Nandra et al. (2005). Briefly, the AEGIS region was targeted over several epochs for a total integration time of 190 ks. Standard reduction methods using the CIAO software were employed to derive fluxes in four energy bands—0.5–7.0 keV (full), 0.5–2.0 keV (soft), 2.0–7.0 keV (hard), and 4.0–7.0 (ultrahard)—by integrating the counts detected within the 70% encircled energy radius at each source position. The counts in each observed band were converted to the standard bands of 0.5–10, 0.5–2, 2–10, and 5–10 keV by assuming an intrinsic power law with  $\Gamma = 1.4$  and Galactic absorption. The typical detection limits in each band are 35, 1.1, 8.2, and 14 in units of  $10^{-16} \text{ ergs s}^{-1} \text{ cm}^{-2}$ , although these depend on position because the *Chandra* sensitivity declines away from the center of each pointing. The full AEGIS-X sample using all eight pointings includes 1318 X-ray detections. These were referenced to the optical/IR photometric catalogs using the method described in Georgakakis et al. (2006).

In terms of the DEEP2 spectroscopic redshifts, target selection was carried out differently in AEGIS than it was in the other DEEP2 fields. Here, a straight magnitude limit of  $R_{AB} \leq 24.1$  was employed with galaxies having  $z \lesssim 0.7$  downweighted but not excluded from the target sample. The near-IR Palomar imaging is deepest in the EGS, especially along the center of the strip where *J*-band imaging was also obtained, and the typical 80% completeness depth is  $K_{AB} = 22.5$ . Overall, the typical AEGIS depth reaches  $K_{AB} \approx 22$ . The properties of the CFHT *BRI* data are identical to those described above.

## 3. THE GALAXY AND AGN HOST SAMPLES

To begin our analysis of AGN hosts and their relationship to evolution in the galaxy population, we distinguish between the *galaxy sample* and the *AGN host sample*. The galaxy sample

comprises the full DEEP2/Palomar survey, including AEGIS. With the goal of providing a self-consistent benchmark for AGN host comparisons, we note that this sample is slightly larger than the one presented in Bundy et al. (2006) because unlike that paper, our analysis does not require that we restrict the perimeter of the survey on account of accurate environmental density measurements. While X-ray observations are not required for the galaxy sample, we do select sources in the  $K_s$  band with good-quality (“z-quality”  $\geq 3$ ; see Davis et al. 2007) spectroscopic redshifts in the redshift range  $0.4 < z < 1.4$ , reaching  $K_s$ -band limits that depend on redshift. As in Bundy et al. (2006), we use  $K_{AB} \leq 21.8, 22.0, 22.2$  for  $z \leq 0.7, 1.0, 1.4$ .

We apply the same limits to the AGN host galaxies, which are identified in the *Chandra* full band and have a Poisson false detection probability that is less than  $4 \times 10^{-6}$ . We then use the redshift of the matched host and assume  $\Gamma = 1.9$  to infer  $L_{2-10}$ , the X-ray luminosity in the 2–10 keV energy band. This effectively corrects for absorption for column densities of  $N_H \lesssim 10^{23} \text{ cm}^{-2}$  at  $z \approx 1$  (Nandra & Pounds 1994), and we apply this procedure even if the source is not detected in the hard band.

AGNs are identified as those sources with  $L_{2-10} > 10^{42} \text{ ergs s}^{-1}$ ; we note that AGNs are certainly present in sources below this threshold, although they are more difficult to distinguish with the present data. Because normal galaxies without AGNs have not been observed with  $L_{2-10} > 10^{42} \text{ ergs s}^{-1}$  (see Bauer et al. 2004), we adopt this limit to ensure that there is little to no contamination from sources without AGNs. Indeed, even without an X-ray luminosity threshold, the flux limit of the *Chandra* data ( $8.2 \times 10^{-16} \text{ ergs s}^{-1} \text{ cm}^{-2}$  in the hard band) suggests a very low non-AGN contamination rate of only a few percent in the observed source densities (Bauer et al. 2004).

While hard X-ray selection provides one of the cleanest ways to select AGNs at high redshift (e.g., Mushotzky 2004; Barger et al. 2005), it still misses Compton-thick sources ( $N_H \gtrsim 10^{24} \text{ cm}^{-2}$ ), which, while not expected to outnumber hard X-ray-detected AGNs, are thought to contribute at least half as many (e.g., Treister et al. 2006; Guainazzi et al. 2005; Gilli et al. 2007). We account for missed Compton-thick AGNs by incorporating the detection efficiency of our sample in the analysis in § 6.

In what follows, we consider the AGN host sample with spectroscopic redshifts and  $R_{AB} \leq 24.1$  (the spec-z sample; 84 sources), as well as a deeper sample ( $R_{AB} \leq 25.1$ ) of AGN hosts supplemented with photometric redshifts (the photo-z sample; 241 sources). As in Bundy et al. (2006), photometric redshifts in AEGIS are estimated using two methods. For galaxies with  $R_{AB} \leq 24.1$  we use ANNz (Collister & Lahav 2004), a neural network redshift estimator, which benefits from a large training set provided by the magnitude-limited nature of the DEIMOS target selection in the EGS. We also include host galaxies with  $24.1 < R_{AB} \leq 25.1$  and  $3 \sigma$  detections in the *BIK* bands, but we use the BPZ SED-based estimator (Benítez 2000) for these sources. By comparing these photo-zs to the DEEP2 spectroscopic redshifts we find  $\delta z/(1+z) = 0.11$ . Further details on these two methods as applied to galaxies in the DEEP2/Palomar sample can be found in Bundy et al. (2006). Photometric redshifts in the EGS based on the CFHT Legacy Survey are also available from Ilbert et al. (2006). Comparing these estimates to the DEEP2 spectroscopic redshifts we find  $\delta z/(1+z) = 0.17$  and therefore use the slightly better ANNz+BPZ estimates described above. Note that Ilbert et al. (2006) redefine  $\delta z/(1+z)$  as  $1.48 \text{median}|z_{\text{spec}} - z_{\text{phot}}|/(1+z_{\text{spec}})$ , and that with this definition the comparison to DEEP2 yields  $d_{z_{\text{Ilbert}}} = 0.03$ , similar to the accuracy reported in Ilbert et al. (2006).

An obvious concern with photometric redshift estimates for AGN hosts is that nonthermal contamination could lead to large

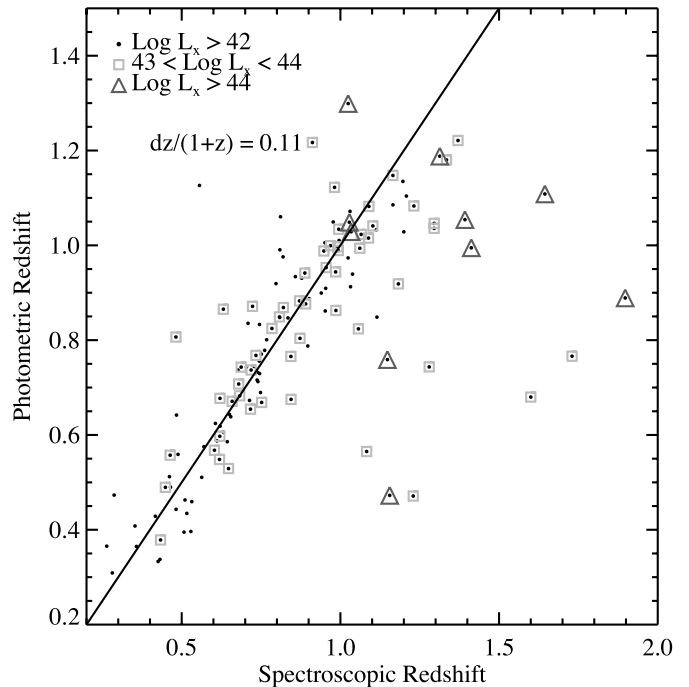


FIG. 1.— Comparison of photo-z quality for the AGN spec-z host sample. Four additional outliers with  $z_{\text{spec}} > 2.0$  are not shown, and all have  $L_{2-10} > 10^{43} \text{ ergs s}^{-1}$ , with three having  $L_{2-10} > 10^{44}$ . As indicated, for  $0.4 < z_{\text{phot}} < 1.4$ ,  $\delta z/(1+z) = 0.11$ , the same as the full galaxy population. We note, however, that photo-z outliers tend to be the most X-ray luminous. [See the electronic edition of the Journal for a color version of this figure.]

redshift errors. By comparing photometric and spectroscopic redshift estimates in the AGN spec-z host sample in Figure 1, we show that in general this is not the case. Since the global sample of galaxies ( $0.4 < z_{\text{phot}} < 1.4$ ) is characterized by the same  $\delta z/(1+z) = 0.11$ , this comparison demonstrates that photometric redshifts of X-ray-selected AGN hosts can be believed at the same level as those of non-AGN galaxies. This implies that AGN contamination in the optical/IR is not significant, as expected (e.g., Barger et al. 2005). Figure 1 does show, however, that the photo-z outliers are dominated by the more X-ray-luminous systems, suggesting more contamination in these cases. Caution must be used in interpreting the properties of these sources. However, we find that excluding the most X-ray-luminous sources ( $L_{2-10} > 10^{44} \text{ ergs s}^{-1}$ ) has a minimal effect on our results and does not change the conclusions of this paper.

## 4. PHYSICAL PROPERTIES

### 4.1. Rest-Frame $U - B$ Color

Following Bundy et al. (2006) and Nandra et al. (2007), we use the methods described in Willmer et al. (2006) to estimate the rest-frame  $U - B$  colors in both our galaxy and AGN host samples. This measurement is frequently used as a diagnostic of star formation activity in galaxies and exhibits a bimodal distribution to at least  $z \sim 1$  (Bell et al. 2004), separating star-forming “blue cloud” galaxies from the mostly passive “red sequence.” We used the cut employed by Willmer et al. (2006), which can be expressed in Vega magnitudes as

$$U - B = -0.032(M_B + 21.52) + 0.454 - 0.25. \quad (1)$$

The  $U - B$  color distribution for the AGN spec-z host sample is illustrated in Figure 2 and was originally discussed for a subset

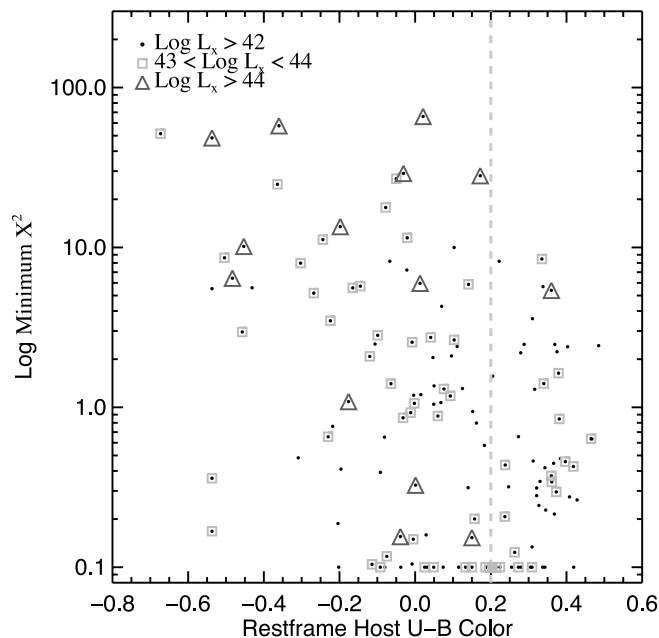


FIG. 2.— Reduced  $\chi^2$  of the best-fitting SED determined by the  $M_*$  estimator as a function of rest-frame ( $U - B$ ) color. More X-ray-luminous AGNs tend to exhibit poorer fits, indicating the presence of AGN contamination. The blue colors of the AGN hosts of X-ray-luminous sources may be caused in part by this contamination. The dashed line is typical of the division used to divide red and blue galaxies. Values of  $\chi^2$  less than 0.1 are plotted as  $\chi^2 = 0.1$ . [See the electronic edition of the *Journal* for a color version of this figure.]

of the data used here in Nandra et al. (2007). The properties of the current and somewhat larger sample here show agreement with those presented in Nandra et al. (2007).

#### 4.2. Stellar Mass Estimates

To estimate stellar masses ( $M_*$ ), we use the methods described in Bundy et al. (2006). Based on the observed *BRICK* colors (measured using  $2.0''$  diameter apertures) and the redshift information for each galaxy, we fit the observed SED to a grid of 13,440 models constructed using the Bruzual & Charlot (2003) population synthesis code. The grid spans a range of metallicities, star formation histories (parameterized as exponential), ages, and dust content. The grid is restricted such that only models with ages (roughly) less than the cosmic age at a galaxy's redshift are considered. Systematic uncertainties are introduced by our choice of a Chabrier IMF (Chabrier 2003) and use of the Bruzual & Charlot (2003) code. While some studies support  $M_*$  estimates based on the Bruzual & Charlot (2003) software (see Kannappan & Gawiser 2007), others have pointed out potential problems (Maraston et al. 2006). In Conselice et al. (2007) we show that a preliminary analysis with the latest G. Bruzual & S. Charlot (2008, in preparation) models yields mass estimates that are  $\sim 0.07$  dex smaller on average. This issue will be discussed further in future work.

With the grid defined in this way, the SED of a given galaxy is then compared to the model at each grid point, where the specific  $K_s$ -band  $M_*/L_K$  ratios and  $M_*$  values for each model are also stored. The probability that each model fits the data is then summed or marginalized over the grid to yield the stellar mass probability distribution. The median of this distribution is taken as the estimate of  $M_*$ , and the width provides an estimate of the uncertainty, typically 0.1–0.2 dex. This is added in quadrature to the  $K_s$ -band magnitude uncertainty to determine the final error on  $M_*$ . Stellar mass estimates for galaxies with only photometric redshifts suffer from the uncertainty in luminosity distance introduced by the

photo- $z$  uncertainties and the possibility of catastrophically wrong redshift information. A study of the effect of photometric redshifts on stellar mass was performed in Bundy et al. (2005).

For the case of the AGN host samples, it is important to consider the effects of nonthermal contamination which may affect the inferred stellar masses. Including an AGN component in the model SEDs used to estimate the stellar mass is not practical. Instead, we investigate the potential error by plotting the reduced  $\chi^2$  values of the best-fitting SED from the stellar mass grid for each member of the AGN spec- $z$  host sample in Figure 2. Even under the best conditions, we do not require a perfect fit to the observed SED because our Bayesian mass estimator considers a range of models when assigning the final mass estimate. Still, mass estimates with  $\chi^2 > 30$  should be considered with caution. Fortunately, while the average  $\chi^2$  value of AGN hosts is higher than for galaxies without AGNs (e.g., the fraction of AGN hosts with  $\chi^2 > 10$  is 10%, while this number for all galaxies is 1%) and seems to correlate with  $L_{2-10}$ , only four hosts have  $\chi^2 > 30$ , indicating that the mass estimates for the AGN host sample are robust.

## 5. STELLAR MASS FUNCTIONS

### 5.1. Methods

With the  $M_*$  estimates described above, we are now in a position to construct stellar MFs from our sample. We describe our formalism in this section and present the AGN host MF in § 5.2. The same methods are also applied to construct MFs for the full galaxy sample. These allow us to study the growing fraction of red galaxies we use to infer the star formation quenching rate in § 6.1.

Constructing galaxy stellar MFs requires understanding and correcting for the limitations and completeness of the survey data. We adopt the  $V_{\max}$  formalism (Schmidt 1968) to this end, following Bundy et al. (2006). In the case of the galaxy sample, the maximum volume can be limited by either the  $K_s$ -band depth or the  $R_{\text{AB}} \leq 24.1$  limit used to define the DEEP2 spectroscopic sample. In this case, for each galaxy  $i$  in the redshift interval  $j$ , the value of  $V_{\max}^i$  is given by the minimum redshift at which the galaxy would leave the sample,

$$V_{\max}^i = \int_{z_{\text{low}}}^{z_{\text{high}}} d\Omega_j \frac{dV}{dz} dz, \quad (2)$$

where  $d\Omega_j$  is the solid angle subtended by the sample defined by the limiting  $K_s$ -band magnitude,  $K_{\text{lim}}^j$  (which changes depending on the redshift interval  $j$ ), and  $dV/dz$  is the comoving volume element. The redshift limits are given as

$$z_{\text{high}} = \min(z_{\text{max}}^j, z_{K_{\text{lim}}}^j, z_{R_{\text{lim}}}), \quad (3)$$

$$z_{\text{low}} = z_{\text{min}}^j, \quad (4)$$

where the redshift interval,  $j$ , is defined by  $[z_{\text{min}}^j, z_{\text{max}}^j]$ ,  $z_{K_{\text{lim}}}^j$  is the redshift at which the galaxy would still be detected below the  $K_s$ -band limit for that particular redshift interval, and  $z_{R_{\text{lim}}}$  is the redshift at which the galaxy would no longer satisfy the  $R$ -band limit of  $R_{\text{AB}} \leq 24.1$ . We use the best-fit SED template as determined by the stellar mass estimator to calculate  $z_{K_{\text{lim}}}^j$  and  $z_{R_{\text{lim}}}$ , thereby accounting for the  $k$ -corrections necessary to compute accurate  $V_{\max}$  values (no evolutionary correction is applied).

In the case of the AGN host samples, the procedure must be modified to account for the limiting X-ray depth. This is more complicated because the limit varies smoothly as a function of position within a given *Chandra* pointing. Deeper sensitivity

limits correspond to smaller effective areas. We therefore compute *Chandra* sensitivity curves in the full band (corresponding to the selection band), accounting for the overlap with the Palomar near-IR data, which is not complete over the EGS field at all depths. For a given source with X-ray luminosity  $L_X^i$ , we use a  $\Gamma = 1.9$  power law to estimate the observed flux this source would have as a function of redshift. We then use the sensitivity curve to compute the corresponding solid angle over which such a source could be detected as a function of redshift,  $d\Omega(z)$ . Thus, we derive a second  $V_{\max}$  estimate for AGN hosts based on the X-ray limits,

$$V_{\max, X\text{-ray}}^i = \int_{z_{\text{low}}}^{z_{\text{high}}} d\Omega(z) \frac{dV}{dz} dz, \quad (5)$$

where  $z_{\text{low}}$  and  $z_{\text{high}}$  are given by the boundaries of the redshift interval. The final  $V_{\max}$  for the AGN hosts is taken as the smaller of the  $V_{\max}$  values computed based on the  $R$ - and  $K_s$ -band limits and  $V_{\max, X\text{-ray}}$ . Typically, the X-ray volume provides the limiting  $V_{\max}$ .

The galaxy sample and AGN spec- $z$  host sample make use of DEEP2 spectroscopic redshifts only. For this reason, additional weights must be applied to account for the redshift targeting selection function and success rate of these samples. Here we follow the technique described by Willmer et al. (2006) and modified in Bundy et al. (2006). Specifically, we compare the number of sources with good-quality redshifts ( $z$ -quality  $\geq 3$ ) in a given bin of  $(B - R)/(R - I)/R_{\text{AB}}/K_s$ -band parameter space to the total number of sources targeted in that same bin. We adopt the “optimal” model of Willmer et al. (2006), which accounts for the different ways that red and blue galaxies are likely to be excluded from the spectroscopic sample.

The situation is more complicated for AGN hosts, because applying this weighting scheme to them assumes that the photometric sources in the corresponding color-magnitude bins also host AGNs. We therefore modify the weighting scheme when it is applied to AGN hosts as follows. In each redshift interval we determine the ratio between the number of spectroscopic AGN hosts and the number of potential hosts. Potential hosts include galaxies without X-ray detections that have spectroscopic redshifts, stellar masses greater than the completeness limit, and  $U - B > -0.1$ . This color requirement is motivated by Figure 2, which demonstrates that most AGN hosts ( $\sim 80\%$ ) have such colors. For the three redshift intervals  $0.4 < z < 0.7$ ,  $0.75 < z < 1.0$ , and  $1.0 < z < 1.4$ , we find AGN fractions of 0.08, 0.09, and 0.14. The AGN spec- $z$  host weights are then determined by multiplying the “optimal” weights discussed above by these numbers and ensuring the weight does not drop below 1.0. No weighting is required for the AGN photo- $z$  host samples; comparisons between the spec- $z$  and photo- $z$  AGN host samples thus provide a useful measure of the success of our weighting scheme.

### 5.2. The AGN Host Stellar Mass Function

We plot the AGN spec- $z$  and photo- $z$  supplemented host MFs in Figure 3 in three redshift intervals. The dark-gray shading represents the uncertainty in the spec- $z$  sample, arising primarily from number statistics. The corresponding MFs of the AGN photo- $z$  host sample are indicated by asterisks connected by dotted lines. For reference, each panel also indicates the total spec- $z$  AEGIS MF (*light-gray shading and filled circles*), the total photo- $z$  supplemented MF (*triangles*), and the best-fitting MF at  $z \approx 0.5$  from Bundy et al. (2006). The number of AGN spec- $z$  hosts diminishes significantly in our highest redshift bin. Interpretations at these redshifts rely on the photo- $z$  sample only. Note that the total photo- $z$  sample covers a larger area (by  $\sim 25\%$ ) than the

spec- $z$  sample. Thus, slight differences in the total MFs can arise from cosmic variance, especially in the lowest redshift interval.

At all redshifts, Figure 3 shows that the AGN host MF is roughly flat across the stellar mass range sampled, consistent with results from the smaller sample of, e.g., Alonso-Herrero et al. (2008). Comparing the AGN photo- $z$  MFs, there is evidence that from  $z \approx 1.2$  to  $\approx 0.5$  the abundance of AGN hosts decreases roughly by a factor of 2 at all stellar masses probed. Because the corresponding number density of all galaxies is lower at  $z \gtrsim 1$ , the fraction of systems hosting AGNs increases at these epochs. This is shown explicitly in Figure 4, which plots the AGN fraction as a function of stellar mass. On one hand, the relatively flat MFs in Figure 3 suggest that AGN evolution—for example, the declining hard X-ray luminosity density (Ueda et al. 2003; La Franca et al. 2005; Barger et al. 2005; Hasinger et al. 2005)—is independent of host  $M_*$  (see Babić et al. 2007). However, the *fraction* of AGN hosts shown in Figure 4 presents a different interpretation. As galaxies continue assembling and their abundance grows with time, X-ray AGNs may be increasingly turning off, especially at the highest masses. This would lead to stronger evolution in the AGN fraction (Fig. 4) accompanied by milder evolution in the absolute numbers of AGN hosts (Fig. 3).

Figure 4 also shows the result of splitting the sample using two different X-ray luminosity thresholds. The dark-gray shading and asterisks denote the AGN host sample with  $L_{2-10} > 10^{42}$  ergs  $s^{-1}$ , as in Figure 3. The light-gray shading and diamonds in Figure 4 provide a comparison to the host MF corresponding to higher X-ray luminosities of  $L_{2-10} > 10^{43}$  ergs  $s^{-1}$ . Note that because of the steep decline in the X-ray luminosity function (LF; e.g., Barger et al. 2005), the AEGIS survey area is too small to effectively sample sources with  $L_{2-10} \gtrsim 10^{44}$  ergs  $s^{-1}$ .

While it appears that the more X-ray-luminous AGNs are generally less abundant, we find little significant difference in the shape of the host MF as a function of X-ray luminosity. Those with  $L_{2-10} > 10^{43}$  ergs  $s^{-1}$  account for roughly one-third of the full AGN sample with  $L_{2-10} > 10^{42}$  ergs  $s^{-1}$  but are associated with host galaxies with a similar mass distribution.

Studies of the AGN X-ray LF show that the more luminous sources are more abundant in the past relative to the less luminous ones, a phenomenon often termed “AGN downsizing” (e.g., Hasinger et al. 2005; Barger et al. 2005). Because this trend is most apparent for systems brighter than the knee in the X-ray LF—that is, AGNs with  $L_{2-10} \gtrsim 10^{44}$  ergs  $s^{-1}$ —we would not expect the effect to be strong in this survey, which is too small to accurately sample such luminous AGNs. There is some suggestion, however, for this effect in the highest mass bin of the  $0.7 < z < 1.0$  redshift interval in Figure 4, where it appears the most massive hosts become dominated by the brightest X-ray AGNs.

## 6. LINKING AGNs AND QUENCHING

We now move to the primary goal of this paper. Our aim is to evaluate the role of AGNs in the evolving star formation properties of the full galaxy population. To accomplish this, we compare the rate at which AGNs are triggered in galaxies of a given mass with the rate at which star formation is quenched at these masses. We use the AGN host MF presented in the previous section (coupled with the AGN lifetime) to infer the AGN trigger rate. First, however, we must characterize the mass-dependent quenching rate in the total population. We use the full Palomar/DEEP2 sample to provide this measurement below.

### 6.1. The Star Formation Quenching Rate

We define the fractional quenching rate,  $\dot{Q}$ , as the fraction of all galaxies in a stellar mass bin that shift to the red sequence per Gyr.

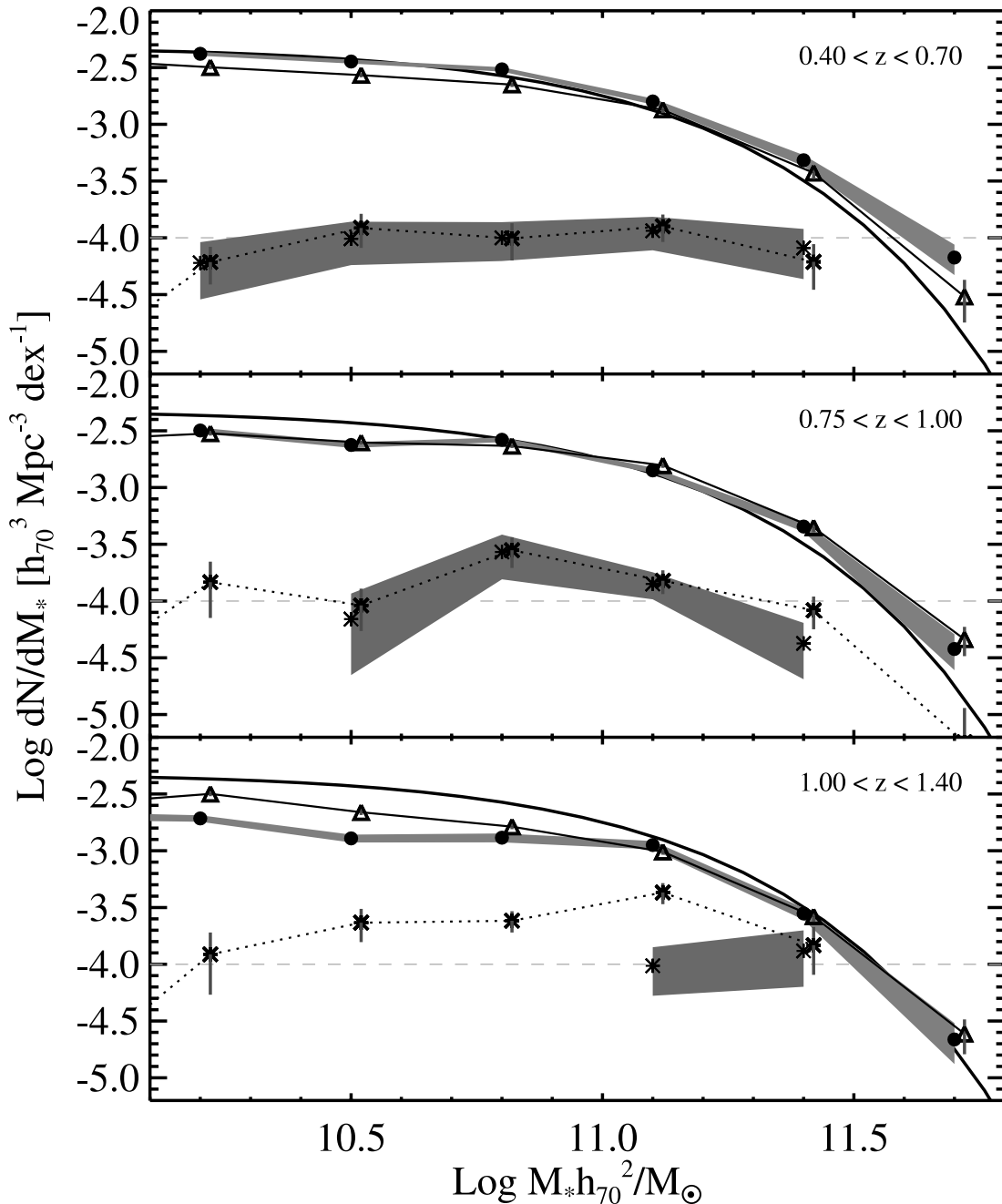


FIG. 3.—Stellar MF of AGN host galaxies in three redshift intervals as compared to the total galaxy stellar MF. Dark-gray shading traces the MF and uncertainty of AGN hosts with spectroscopic redshifts and  $L_{2-10} > 10^{42}$  ergs  $s^{-1}$ . The asterisks with error bars connected by the dotted line show the AGN host MF for the photo- $z$  supplemented sample. Total MFs from the AEGIS field are shown with circles and light-gray shading (spec- $z$  sample) and triangles (photo- $z$  supplemented sample). The solid line is taken from the best fit of Bundy et al. (2006) to the total MF at  $z \approx 0.5$ . A dashed line has been drawn at  $\phi = 10^{-4}$  in all panels to guide the eye. [See the electronic edition of the Journal for a color version of this figure.]

This quantity can be derived using the methods of § 5 to plot the increasing fraction of red galaxies (relative to the abundance of all galaxies) as a function of time for various bins of stellar mass (Fig. 5). We use the slope of the increasing red fraction to estimate  $\dot{Q}$ . We have chosen to study the red galaxy fraction, as opposed to absolute number densities, because this helps mitigate uncertainties caused by cosmic variance, which to first order affect the total number density measured in a given redshift interval (see Bundy et al. 2006).

The use of fractional abundances also provides a better handle on the rate at which galaxies become red, that is,  $\dot{Q}$ . In the absence of processes that shift galaxies into different mass bins,

quenching only alters the fraction of red galaxies in a given  $M_*$  bin. The transfer of galaxies across mass bins is constrained to be small by the lack of significant evolution in the shape of the total MF from  $z \sim 1$ . However, it is possible that both star formation and merging may move galaxies between mass bins. As for merging, we make the assumption that the effect on the red fraction is small if merging is independent of galaxy type and the merging rate does not vary across the 0.3 dex mass bins used here. As for star formation, because lower mass galaxies exhibit higher star formation rates, their evolution would tend to drive the red fraction down as low-mass blue galaxies enter a given mass bin. However, as the number of galaxies forming stars at a rate sufficient to

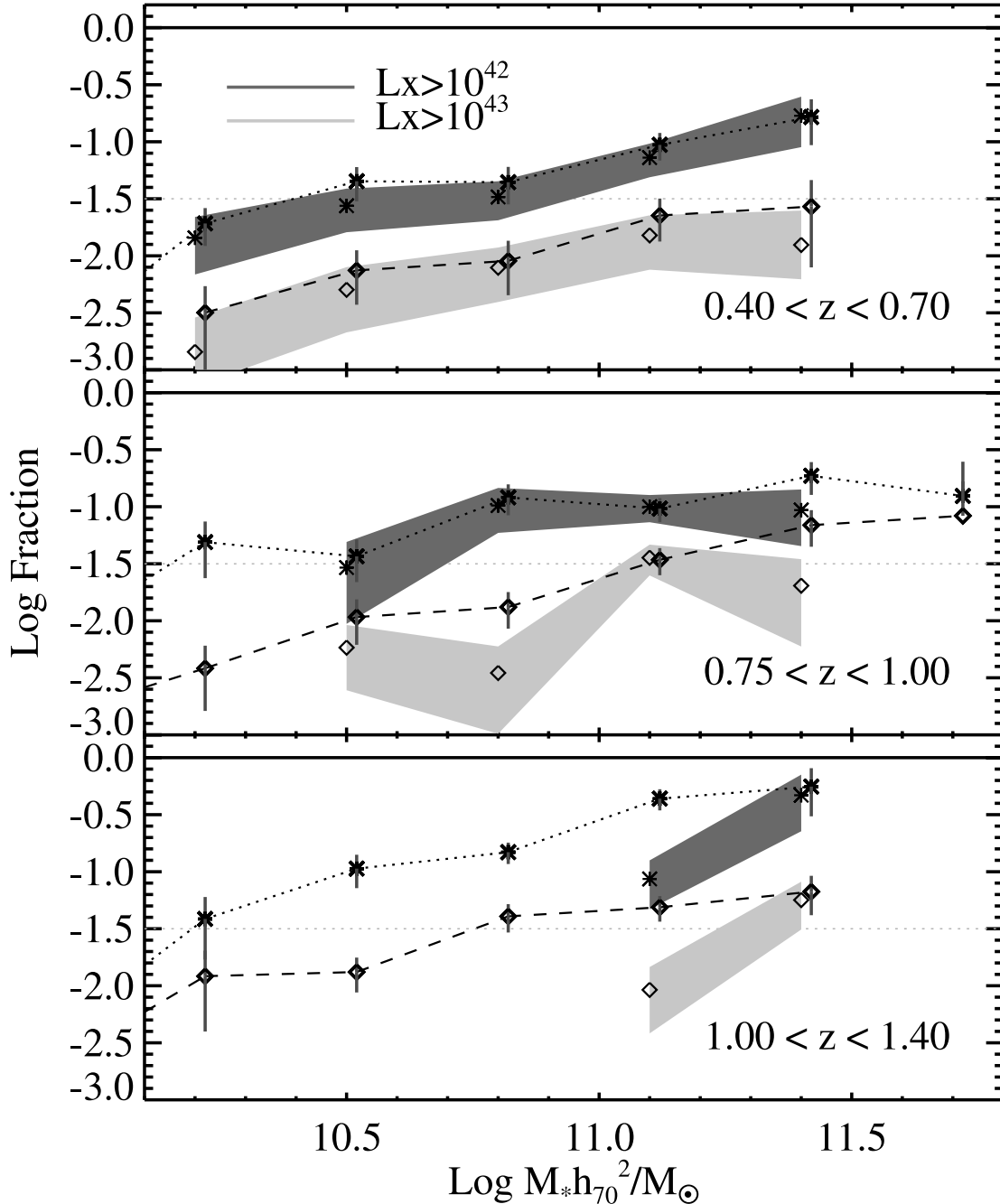


FIG. 4.—Fractional contribution of AGN hosts to the total MF in log units, shown in three redshift intervals. As in Fig. 3, dark-gray shading denotes the AGN spec-z host sample with  $L_{2-10} > 10^{42}$  ergs  $s^{-1}$ , while asterisks connected by dotted lines denote the AGN photo-z host sample with the same  $L_{2-10}$  threshold. Light-gray shading corresponds to AGN spec-z hosts with the brighter X-ray cut of  $L_{2-10} > 10^{43}$  ergs  $s^{-1}$ , while diamonds connected by dashed lines show the corresponding AGN photo-z MFs. A dotted line at  $\log f = -1.5$  has been drawn in each panel to guide the eye. [See the electronic edition of the Journal for a color version of this figure.]

double their mass over a few Gyr is small for  $M_* \gtrsim 10^{10} M_\odot$  (e.g., Feulner et al. 2005), such an effect would have a small impact on the red fraction. Still, we emphasize that the evolving red fraction in specific mass bins is only an estimate of the true quenching rate.

The buildup in the fraction of red systems is clear in Figure 5 and allows us to crudely fit lines to the fractional growth rate in each mass bin. In these fits, we exclude points at early times and low masses that fall below our expected completeness limit, as well as those points for which the red fraction is equal to 1.0. We take the slope of these lines as our estimate of  $\dot{Q}$  at each mass. In the mass bins centered at  $\log M_*/M_\odot = 10.5, 10.8, 11.1, 11.4,$  and  $11.7$  we find fractional quenching rates,  $\dot{Q}(M_*)$ , of  $8\% \pm 3\%$ ,

$9\% \pm 3\%$ ,  $11\% \pm 3\%$ ,  $16\% \pm 6\%$ , and  $28\% \pm 23\%$  per Gyr. While Figure 5 shows that our linear approximation adequately fits the data, we cannot further constrain the quenching rates as a function of time (or redshift). Our results are obviously only valid until the red fraction reaches 1.0 and all systems are quenched, and, extrapolating the fits, we find that “total quenching” in these mass intervals occurs when the cosmic age  $\tau_{\text{age}} = 14.7, 11.4, 9.3, 7.5,$  and  $7.3$  Gyr. Figure 5 not only reinforces the notion that more massive galaxies become quenched first but suggests the new result that they may also become quenched *faster* than their lower mass counterparts. We note, however, that the uncertainties on our mass-dependent quenching rates are large;

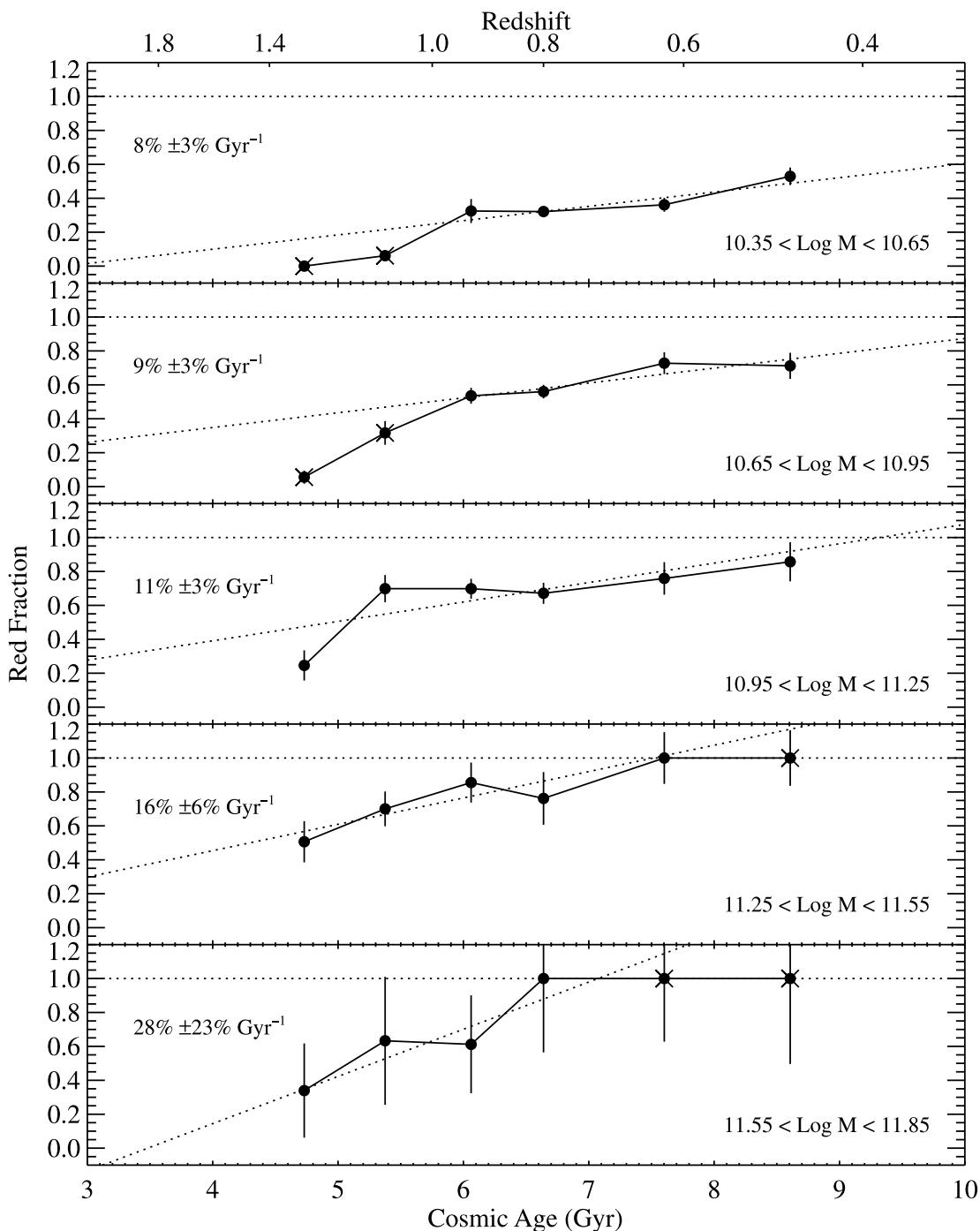


FIG. 5.—Evolving fraction of red galaxies as a function of time in various mass bins. The growing fractions have been fit by the dotted lines, excluding data points where either the fraction is 1.0 or the data are incomplete. Excluded data points are indicated by crosses.

the apparent trend of higher quenching rates for more massive galaxies is significant at the  $\approx 1.3 \sigma$  level.

### 6.2. Comparing AGN Triggering and Star Formation Quenching

With the star formation quenching rate measured above, we now use the AGN host MF to derive the AGN “trigger rate,”  $\dot{\chi}(M_*)$ , defined as the fraction of all galaxies per Gyr in which X-ray-detected AGNs turn on as a function of stellar mass. The rate of AGN triggering multiplied by the timescale over which AGNs are visible at X-ray wavelengths is equal to the observed AGN fraction (shown in Fig. 4). If we account for the AGN

detection efficiency,  $\epsilon$ , of our X-ray observations, we can write this relation as  $f_{\text{AGN}}(M_*) = \epsilon \dot{\chi}(M_*) \tau_{\text{AGN}}$ , where  $\tau_{\text{AGN}}$  is the X-ray AGN timescale.

This timescale is the largest uncertainty in the calculation and must be derived from theoretical arguments. We consider three estimates taken from the literature for the average value of  $\tau_{\text{AGN}}$ . From the detailed simulations studied in Hopkins et al. (2005b) we find  $\tau_{\text{AGN}} \approx 0.6$  Gyr. From the statistical and population arguments for low-efficiency AGNs in Marconi et al. (2004) we use  $\tau_{\text{AGN}} \approx 0.9$  Gyr, and from the model discussed in Granato et al. (2004) we use  $\tau_{\text{AGN}} \approx 1.8$  Gyr. We return to the timescale problem and discuss these estimates further below.

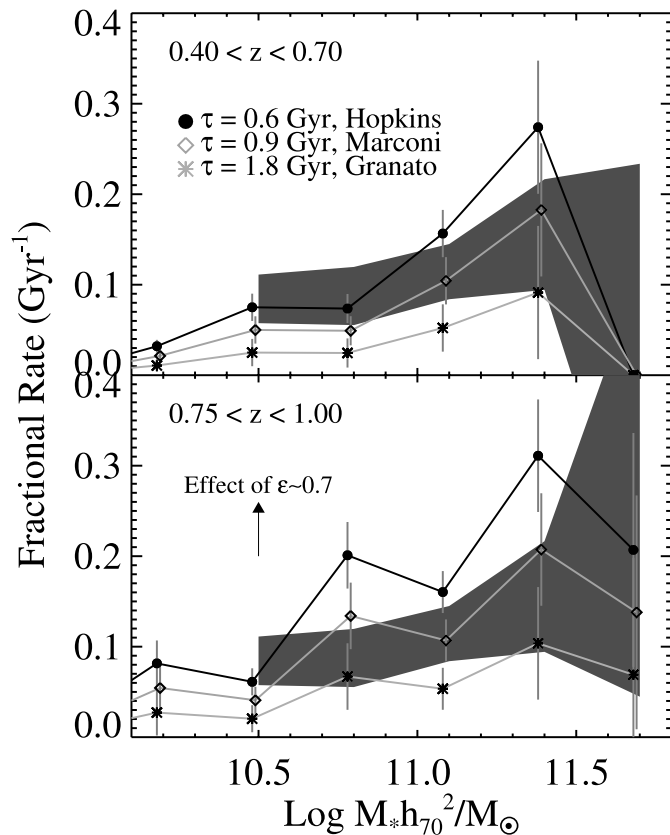


FIG. 6.—Comparison in two redshift bins of the fractional AGN “trigger rates” calculated using three estimates of the X-ray AGN timescale and the star formation quenching rate (*shaded region*). The width of the shading illustrates the  $1\sigma$  uncertainty. Trigger rates are derived based on the AGN photo- $z$  sample (similar results are obtained for the spec- $z$  sample), assuming all AGNs are detected and X-ray AGN timescales of 0.6, 0.9, and 1.8 Gyr based on estimates from the work of Hopkins et al. (2005b), Marconi et al. (2004), and Granato et al. (2004). The systematic effect of a 70% detection efficiency ( $\epsilon \approx 0.7$ ) is shown by the arrow. [See the electronic edition of the *Journal* for a color version of this figure.]

Assuming  $\epsilon = 1$ , we solve for the corresponding trigger rates,  $\dot{\chi}(M_*)$ , by dividing the AGN host fraction ( $L_{2-10} > 10^{42}$ ; Fig. 4) by the timescales above. We plot the results for the two redshift bins in which our sample is most complete in Figure 6. The corresponding star formation quenching rate from our analysis of red galaxies is denoted by the gray shaded region. The effect of a lower detection efficiency of  $\epsilon \approx 0.7$  arising from missed Compton-thick sources, as estimated by Treister et al. (2006), increases the trigger rates, as roughly shown by the arrow.

Despite the uncertainties and assumptions, Figure 6 demonstrates surprising agreement in both the normalization and mass dependence of the rates of quenching and AGN triggering, given the three estimates for  $\tau_{\text{AGN}}$ . We interpret this as strong but circumstantial evidence that the quenching of star formation and AGN activity are physically related. We turn to the question of whether AGNs actually *cause* quenching in § 6.4.

### 6.3. The X-Ray AGN Timescale

Because the calculation of the AGN trigger rates shown in Figure 6 relies heavily on the assumed value of  $\tau_{\text{AGN}}$ , in this section we further explore the X-ray AGN timescale and the reliability of the estimates we have used. As a point of reference, we begin by deriving the value of  $\tau_{\text{AGN}}$  that would be necessary to *force* the observed quenching and triggering rates to be equal. We set  $\dot{Q}(M_*) = \dot{\chi}(M_*)$  and solve for  $\tau_{\text{AGN}}$  at each stellar mass bin where estimates of the two rates are available (essentially, we

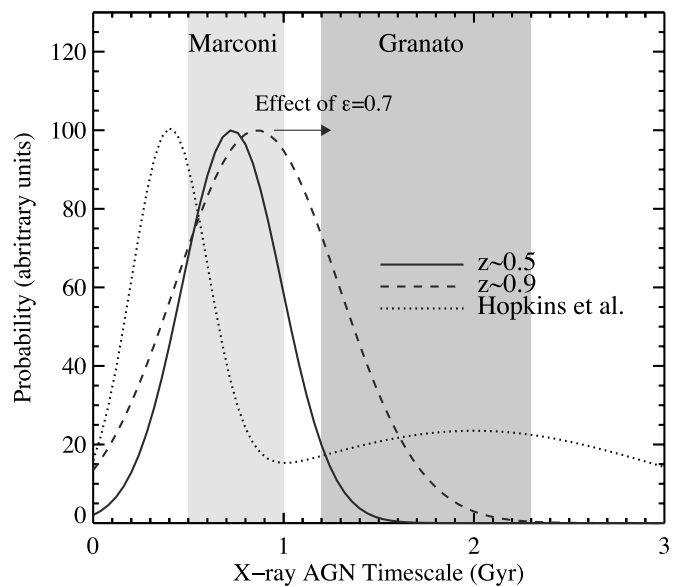


FIG. 7.—Range of X-ray-detectable AGN timescales. As a reference point, the result of *assuming* the AGN trigger rate equals the quenching rate yields timescales in the range indicated by the solid ( $z \sim 0.5$ ) and dashed ( $z \sim 0.9$ ) distributions. The effect of a 70% AGN detection efficiency ( $\epsilon = 0.7$ ) on these distributions is shown by the arrow. Independent predictions of  $\tau_{\text{AGN}}$  based on the models of Hopkins et al. (2005b) have a range indicated by the dotted line. Predictions from Granato et al. (2004) and Marconi et al. (2004) are denoted by the shaded regions. [See the electronic edition of the *Journal* for a color version of this figure.]

divide the full AGN host fraction in Fig. 4 by the quenching rates derived in Fig. 5). In principle,  $\tau_{\text{AGN}}$  may be related to the host stellar mass, but we ignore this and average over the values of  $\tau_{\text{AGN}}$  derived for each mass bin to roughly estimate the range or “probability distribution” of timescales needed to perfectly match the quenching and AGN trigger rates observed in our two redshift intervals. These are plotted in Figure 7 (*solid and dashed lines*) and illustrate where theoretical estimates of  $\tau_{\text{AGN}}$  would fall if it were true that  $\dot{Q}(M_*) = \dot{\chi}(M_*)$ .

We can now compare the estimates of  $\tau_{\text{AGN}}$  we have used and discuss their uncertainties. The most appropriate predictions come from detailed simulations analyzed by Hopkins and collaborators. Hopkins et al. (2005b) conduct five hydrodynamical simulations of gas-rich mergers of disk galaxies that host supermassive black holes (SMBHs). During the simulations, gas becomes funneled to the center of the system, fueling the growth of the newly merged SMBH. The authors use a prescription in which some fraction ( $\epsilon_r = 0.1$ ) of this accreted material is radiated in a quasar phase. They assume that 5% of this energy couples with the surrounding gas, helping to regulate the flow. The X-ray luminosity (and column density) as a function of time is calculated by assuming a quasar continuum SED and ray-tracing many lines of sight through the gas and dust in the simulated galaxy. Their Figure 2 presents a relation between the observed AGN lifetime ( $\tau_{\text{AGN}}$ ) and its X-ray luminosity. By applying this relation to the X-ray luminosities observed in our sample we derive a rough distribution of predicted AGN timescales, which we plot in Figure 7 (*dotted line*). Note that the predicted  $\tau_{\text{AGN}}$  from the Hopkins et al. (2005b) models increases rapidly for AGNs with  $L_X \lesssim 5 \times 10^{42}$  ergs s $^{-1}$ , accounting for the tail toward longer lifetimes shown in the figure and yielding the estimate of  $\tau_{\text{AGN}} \approx 0.6$  Gyr used in Figure 6.

The work of Granato et al. (2004) provides another independent comparison, also based on numerical simulations that encode the effects of star formation, cooling, supernova feedback, and AGN feedback set in the context of dark matter halos. The

systems analyzed in Granato et al. (2004) are noninteracting spheroidal galaxies as opposed to merging disks, however, and while the simulations lack detailed modeling of the AGN X-ray emission, some rough constraints can be obtained for the predicted values of  $\tau_{\text{AGN}}$ . Their Figure 3 shows the black hole accretion rate as a function of cosmic time in their simulations. Since, as we show below, our AGNs are likely accreting at significantly sub-Eddington rates, a rough estimate of  $\tau_{\text{AGN}}$  from Granato et al. (2004) can be gained by measuring the time between peak black hole accretion in their simulations and the point at which the accretion drops below a factor of 0.01–0.001 of the maximum rate. This yields AGN timescales between  $\sim 1$  and  $\sim 2$  Gyr, as shown in Figure 7 (*gray shaded region*). For an average value from Granato et al. (2004) we take  $\tau_{\text{AGN}} \approx 1.8$  Gyr.

Finally, much work has been invested in using various observations to constrain the lifetime of bright quasar activity, typically resulting in values of  $10^7$ – $10^8$  yr (see the review by Martini 2004). However, historically the focus has rested on the brightest quasar phase, during which black hole growth is thought to be most rapid. This phase does not correspond to the lower accretion rates of the AGNs detected in our sample. Marconi et al. (2004), however, provide a suitable estimate based on matching the local black hole density to the AGN LF. For low-efficiency sources, the predicted range is  $\tau_{\text{AGN}} \approx 0.5$ – $1$  Gyr, weighted more toward 1 Gyr for the lowest luminosity AGNs and providing a rough average value of  $\tau_{\text{AGN}} = 0.9$  Gyr.

It is clear from Figure 7 that large uncertainties exist. Still, from the detailed analysis in Hopkins et al. (2005b) to the more approximate estimates from Marconi et al. (2004) and Granato et al. (2004), this plot demonstrates that the predicted range and uncertainty in the timescale for X-ray AGN activity using a variety of methods is at least compatible with a scenario in which AGN triggering is linked to quenching. This helps validate the agreement seen in Figure 6. Clearly, further progress in confirming this link would strongly benefit from additional detailed predictions of the X-ray properties and lifetimes of AGNs.

#### 6.4. Is AGN Feedback Responsible for Quenching?

We have argued that the similarity in the rate of AGN triggering compared to the rate of star formation quenching suggests that the two phenomena are linked. But what is the nature of this link? Specifically, we would like to know whether AGNs, perhaps through feedback mechanisms, are directly responsible for the quenching of star formation. In this section we begin to probe this question by investigating the individual properties of our X-ray-selected AGNs and how they correlate with their host galaxies.

Our strategy is to study the SMBH accretion rates as parameterized by the Eddington ratio in our sample. We acknowledge that these estimates are somewhat crude and subject to systematics but argue that they nonetheless provide important insight on how AGNs are related to the properties of their host galaxies. The Eddington ratio compares the bolometric luminosity,  $L_{\text{bol}}$ , of the AGN to the Eddington luminosity, which is simply related to the SMBH mass,  $L_{\text{Edd}} = 1.25 \times 10^{38} (M_{\text{BH}}/M_{\odot}) \text{ ergs s}^{-1}$ . To determine  $M_{\text{BH}}$  we use the relation between  $K$ -band bulge luminosity and black hole mass calculated by Graham (2007) and based on previous work (Marconi & Hunt 2003; McLure & Dunlop 2004). Note that Woo et al. (2006) find evidence that the  $z \sim 0.3$  relation is offset relative to that at  $z = 0$  by a +0.6 dex increase in  $M_{\text{BH}}$ , although we do not apply this correction here. As most X-ray-selected AGN hosts at the redshifts of our sample have early-type morphologies (Grogin et al. 2005; Pierce et al. 2007), we assume that the bulge-to-total ratio is 1.0, but in what

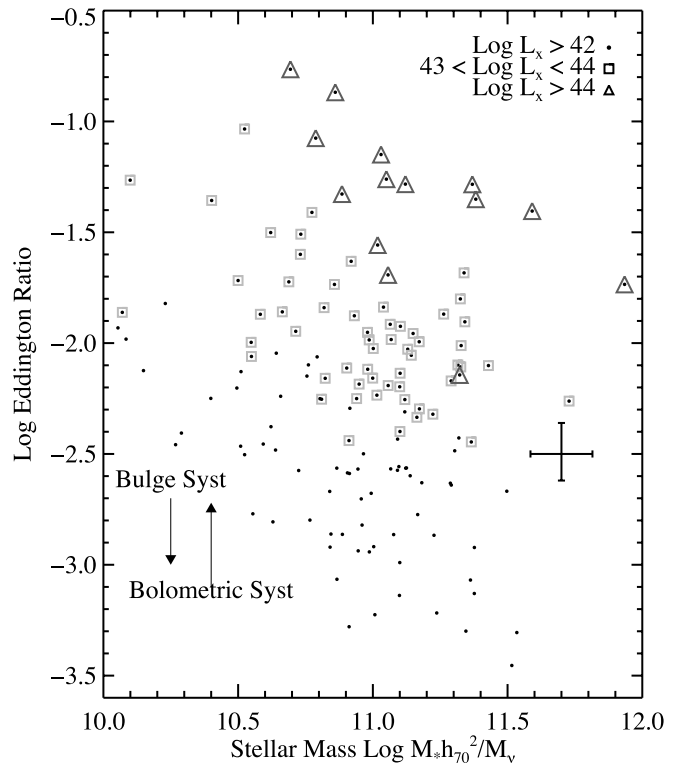


FIG. 8.—Eddington ratios in the AEGIS spec- $z$  sample plotted against the host galaxy stellar mass. Different symbols indicate different ranges of AGN X-ray luminosity as shown. The isolated error bar illustrates the typical uncertainty arising from observational scatter. The labeled arrows suggest the magnitude and sense of systematic uncertainties. The “bulge” systematic shows what would happen if the applied value of  $M_{\text{BH}}/M_{\text{bulge}}$  was increased by a factor of 2. Lowering the bulge-to-total ratio by the same amount has the equivalent effect in the opposite direction. The “bolometric” systematic shows the effect of increasing the bolometric correction from 35 to 85. Note that the axes are not fully independent because the Eddington ratio is proportional to  $M_{*}^{-1}$ , leading to the slight downward trend observed. [See the electronic edition of the *Journal* for a color version of this figure.]

follows we demonstrate the effect of lower ratios on our results. Finally, we calculate  $L_{\text{bol}}$  by assuming a hard X-ray bolometric correction of 35 (Elvis et al. 1994). Barger et al. (2005) argue that for obscured (narrow-line) AGNs, the correction should be 85, although Pozzi et al. (2007), using a sample of type 2 AGNs, find a wide range of bolometric corrections with an average of  $\sim 25$ . Clearly, the bolometric corrections are uncertain within a factor of  $\sim 2$ – $3$ .

Using the methods above and with the stated caveats in mind, we plot the estimated Eddington ratio as a function of stellar mass in Figure 8. The X-ray luminosity range of the data is indicated, showing that more luminous AGNs tend to have more efficient accretion. The isolated error bar indicates the typical uncertainties from observational scatter, while the arrows show the effects of systematic errors in estimating the bulge luminosity and bolometric correction. The “bulge” systematic shows how the estimate of  $L_{\text{Edd}}$  decreases if the applied value of  $M_{\text{BH}}/M_{\text{bulge}}$  is increased by a factor of 2. Lowering the bulge-to-total ratios by the same amount has the equivalent effect in the opposite direction, increasing  $L_{\text{Edd}}$ . The “bolometric” systematic shows the effect of increasing the bolometric correction from 35 to 85. It is important to note that our calculation of the Eddington ratio ensures that it is proportional to  $M_{*}^{-1}$  (since  $L_{\text{Edd}} \propto M_{\text{BH}}^{-1}$ ), so downward mass-dependent trends in Figure 8 are expected given our methodology.

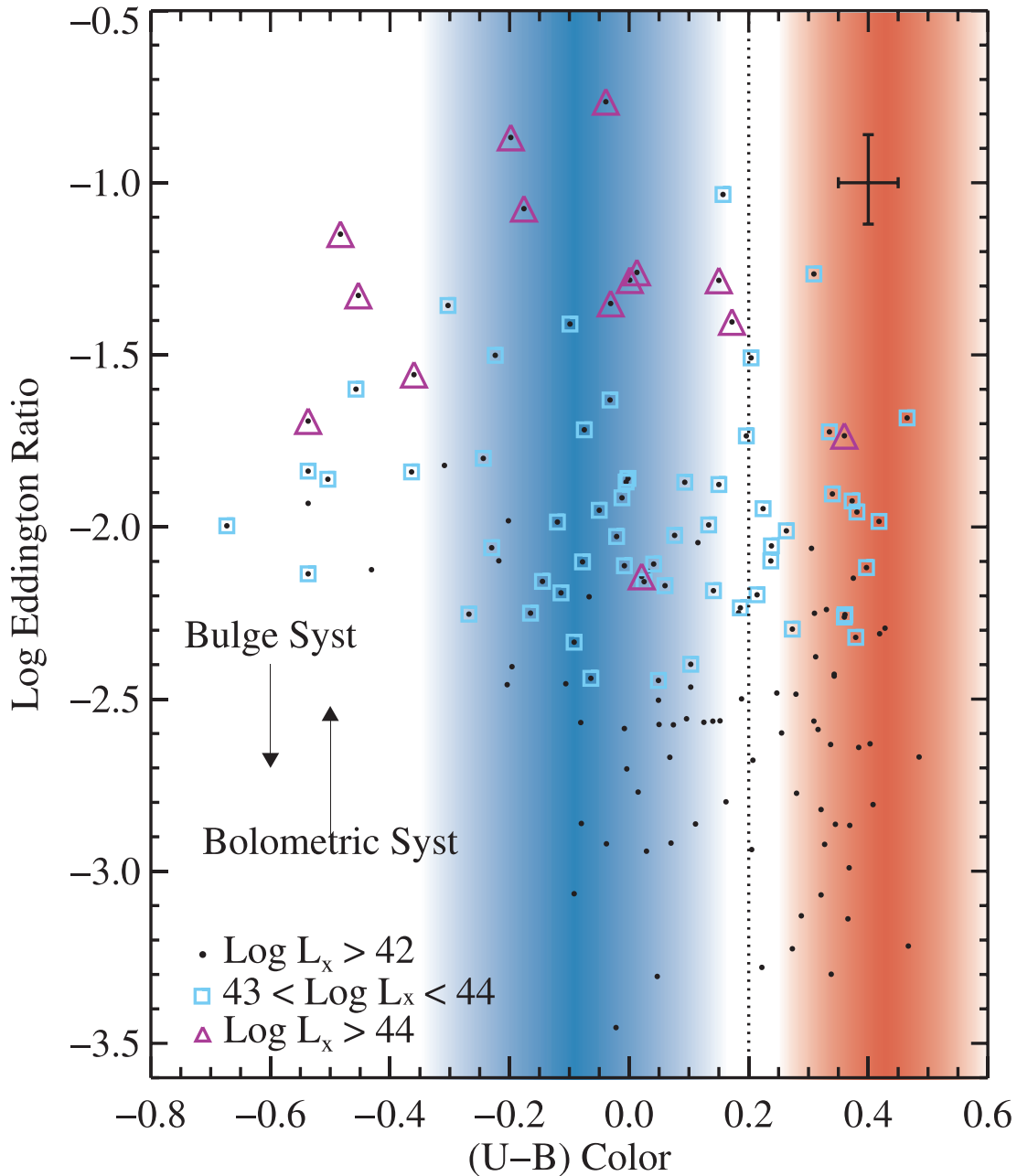


FIG. 9.—Eddington ratios as in Fig. 8 for host galaxies of varying rest-frame  $(U - B)$  color. A typical value for the division between red and blue galaxies is shown by the dotted line, and the color distributions of all galaxies are indicated by the background blue and red shading.

What is perhaps most revealing about the figure, however, is the large range (more than 2 orders of magnitude) in Eddington ratios that is apparent for host galaxies of all masses. Figure 9 shows a similar diagram where it is now possible to compare the Eddington ratios versus host galaxy rest-frame  $U - B$  color. The red and blue distributions of all galaxies are indicated by the background shading. Note the existence of very blue hosts (beyond the range of normal colors) dominated by bright X-ray systems. As observed in Nandra et al. (2007), it is likely that the AGN contaminates the host color of these galaxies.

Considering the hosts in the blue cloud and red sequence, there appears to be little difference in the large spread of accretion rates. This is especially the case when one ignores the X-ray-brightest systems (Fig. 9, *triangles*), whose true host colors may be redder than observed. We note that among all galaxies at  $z \approx 0$ , the fraction of dusty but still star-forming systems on the

red sequence is  $\sim 7\%$  and is not likely to be significantly higher at  $z \sim 1$  (Yan et al. 2006). It is therefore likely that most red AGN hosts in Figure 9 are truly quenched systems.

While the uncertainties in Figures 8 and 9 are large, the intrinsic scatter appears to be more substantial and suggests few or no additional trends with stellar mass or color beyond those expected from the methodology. These observations may therefore have important implications for the question of whether AGN feedback is responsible for quenching.

Some feedback models imagine that the AGN has an explosive episode that drives gas out of the galaxy halo. In the model of Hopkins and collaborators discussed above, for example, AGN activity is triggered by major mergers. The buried AGN is virtually undetectable until a violent quasar phase in which tremendous energy is expelled, sufficient to heat or dispel most of the remaining gas in the galaxy, thus quenching further star

formation. As described in Hopkins et al. (2008b), in this model one would expect that AGN activity evolves with time as AGN feedback during the quasar phase impacts the surrounding material, heating and driving it from the newly merged system. The X-ray observations studied here would then correspond to the postquasar phase tracing AGNs as they decay to low luminosities; beforehand, the obscuration is predicted to be  $\geq 10^{24} \text{ cm}^{-2}$ , enough to absorb hard X-rays. The short-lived quasar phase that immediately follows would be too bright to enable studies of host properties (see Hopkins et al. 2008b).

Figures 8 and 9 suggest some potential problems with simple interpretations of explosive models of this sort. One might expect the most massive and reddest hosts to have been quenched earliest and therefore to harbor AGNs in the latest stages of decay. Little fuel should remain in such systems long after the quasar phase, and the luminosities and Eddington ratios should be low. This picture appears consistent with observations of local AGN hosts identified through optical emission-line diagnostics. Stronger emission-line AGNs are found in younger stellar populations with higher specific star formation rates, while weaker AGNs favor hosts that have apparently been quenched (Kauffmann et al. 2003; Salim et al. 2008; Schawinski et al. 2007). Figures 8 and 9 show that X-ray-selected AGNs may present a different picture. Here, the reddest and most massive hosts harbor AGNs that cover nearly the full range of X-ray luminosity and accretion rates. Indeed, Figure 3 demonstrates that AGNs are hosted by galaxies with masses covering the full range probed.

One perspective on this question is suggested by the work of Ciotti & Ostriker (2007), who demonstrate that X-ray-luminous AGN activity, as well as starbursts, can be effectively fueled by stellar mass loss from evolved stars in old stellar populations. While it is not clear what timescales would be involved, in the absence of other fueling mechanisms, this process requires an old stellar population to function, generating an obvious link between quenching and the appearance of AGNs. The work of Ciotti & Ostriker (2007) serves to demonstrate that AGNs may be fueled by a variety of mechanisms. Even if a high-accretion quasar phase was initially responsible for disrupting the internal gas supply, the AGN may later be “refueled” by such mechanisms, including the inflow of gas lost from evolved stars.

Finally, in addition to refueling, an alternative explanation for the range of AGN properties observed in the most massive and reddest hosts could come from the notion that AGN feedback is *not* responsible for quenching star formation but is triggered by the same process that is. A nuclear starburst fueled by the same inflowing gas that ignites the AGN is a promising example, capable of providing the feedback energy necessary (in the form of stellar winds) to heat and expel the surrounding gas supply and help regulate correlations between bulge and SMBH properties (see Ferrarese & Ford 2005). Previous work has revealed evidence for a connection between starbursts and AGN activity (e.g., Yan et al. 2006; Goto 2006; Yang et al. 2006; Wild et al. 2007; Georgakakis et al. 2008) which has also been explored in models (e.g., Somerville et al. 2001; Hopkins et al. 2008a).

A mixed AGN/starburst scenario is supported by the observations presented here. AGN activity could be initially triggered during or toward the end of starburst quenching, leading to a greater diversity in the phases of X-ray-detected AGN activity among galaxy hosts. As suggested by Croton et al. (2006), low-luminosity AGNs, undetected in the current sample, may be ubiquitous in quenched systems (e.g., Salim et al. 2008), providing the necessary feedback that prevents further star formation. As part of this feedback cycle, these systems could

periodically enter active phases that could be detected through X-ray emission.

## 7. SUMMARY

We have used the combination of the DEEP2 Galaxy Redshift Survey, Palomar near-IR imaging, and *Chandra* X-ray observations to study the properties of galaxies that host X-ray-selected AGNs. We summarize our findings below.

1. The AGN host stellar mass function (MF) over the redshift range  $0.4 < z < 1.4$  is roughly flat as a function of  $M_*$ . The abundance of AGNs appears higher at  $z \sim 1$  by a factor of  $\sim 2$ . Coupled with the decrease in number density of all galaxies at high redshift, the AGN fraction increases at early times, especially among the most massive galaxies.

2. The MF of host galaxies for an X-ray-luminous subset of our sample with AGN luminosities of  $L_{2-10} > 10^{43} \text{ ergs s}^{-1}$  indicates a lower abundance but a mass dependence very similar to that of the full sample with  $L_{2-10} > 10^{42} \text{ ergs s}^{-1}$ . We see some evidence, however, that brighter AGNs, whose abundance increases with redshift, are hosted by more massive galaxies.

3. Using the full DEEP2/Palomar sample we estimate the star formation quenching rate, defined as the number of galaxies that move to the red sequence per Gyr. Our estimates suggest that massive galaxies not only populated the red sequence at earlier epochs but did so at a faster rate than less massive galaxies.

4. We show that the quenching rate agrees with the rate at which AGN activity is triggered in galaxies if the AGN detection efficiency is  $\sim 70\%$  and the lifetime of AGN activity is  $\sim 1$  Gyr. This timescale is similar to estimates from detailed predictions based on numerical simulations and black hole demographics. The agreement between the mass-dependent quenching and AGN triggering rates is evidence of a physical link between these two phenomena.

5. We test the causality of this link by comparing black hole accretion rates to the stellar mass and color of associated host galaxies. The most massive and red hosts, which presumably were quenched at the earliest times, harbor X-ray-selected AGNs as active as those found in blue hosts. This suggests a more complicated relationship between AGNs and star formation. It is possible that X-ray-selected AGNs are associated with but do not directly *cause* star formation quenching and, furthermore, may be subject to refueling after quenching occurs.

We would like to thank Ray Carlberg for useful discussions on this project. K. B. would like to acknowledge support from Olivier Le Fèvre and the Observatoire Astronomique de Marseille Provence, where he was a visiting researcher. The Palomar Survey was supported by National Science Foundation grant AST 03-07859 and NASA STScI grant HST-AR-09920.01-A. Support from NSF grants 00-71198 to the University of California, Santa Cruz, and AST 00-71048 to the University of California, Berkeley, is also gratefully acknowledged. Financial support has also been provided through PPARC and the Marie Curie Fellowship grant MEIF-CT-2005-025108 (A. G.), the Leverhulme trust (K. N.), the Hubble Fellowship grants HF-01165.01-A (J. A. N.) and HF-01182.01-A (A. L. C.), and the STFC (E. L.). We wish to recognize and acknowledge the highly significant cultural role and reverence that the summit of Mauna Kea has always had within the indigenous Hawaiian community. It is a privilege to be given the opportunity to conduct observations from this mountain.

## REFERENCES

- Alonso-Herrero, A., Perez-Gonzalez, P. G., Rieke, G. H., Alexander, D. M., Rigby, J. R., Papovich, C., Donley, J. L., & Rigopoulou, D. 2008, *ApJ*, 677, 127
- Babić, A., Miller, L., Jarvis, M. J., Turner, T. J., Alexander, D. M., & Croom, S. M. 2007, *A&A*, 474, 755
- Barger, A. J., Cowie, L. L., Mushotzky, R. F., Yang, Y., Wang, W.-H., Steffen, A. T., & Capak, P. 2005, *AJ*, 129, 578
- Bauer, F. E., Alexander, D. M., Brandt, W. N., Schneider, D. P., Treister, E., Hornschemeier, A. E., & Garmire, G. P. 2004, *AJ*, 128, 2048
- Bell, E. F., et al. 2004, *ApJ*, 608, 752
- Benitez, N. 2000, *ApJ*, 536, 571
- Bertin, E., & Arnouts, S. 1996, *A&AS*, 117, 393
- Borch, A., et al. 2006, *A&A*, 453, 869
- Bower, R. G., et al. 2006, *MNRAS*, 370, 645
- Bruzual, G., & Charlot, S. 2003, *MNRAS*, 344, 1000
- Bundy, K., Ellis, R. S., & Conselice, C. J. 2005, *ApJ*, 625, 621
- Bundy, K., et al. 2006, *ApJ*, 651, 120
- Canalizo, G., & Stockton, A. 2001, *ApJ*, 555, 719
- Cattaneo, A., Dekel, A., Devriendt, J., Guiderdoni, B., & Blaizot, J. 2006, *MNRAS*, 370, 1651
- Chabrier, G. 2003, *PASP*, 115, 763
- Cimatti, A., Daddi, E., & Renzini, A. 2006, *A&A*, 453, L29
- Ciotti, L., & Ostriker, J. P. 2007, *ApJ*, 665, 1038
- Coil, A. L., Newman, J. A., Kaiser, N., Davis, M., Ma, C.-P., Kocevski, D. D., & Koo, D. C. 2004, *ApJ*, 617, 765
- Collister, A. A., & Lahav, O. 2004, *PASP*, 116, 345
- Conselice, C. J., et al. 2007, *MNRAS*, 381, 962
- Cooper, M. C., et al. 2007, *MNRAS*, 383, 1058
- Cowie, L. L., Songaila, A., Hu, E. M., & Cohen, J. G. 1996, *AJ*, 112, 839
- Croton, D. J., et al. 2006, *MNRAS*, 365, 11
- Cuillandre, J.-C., Luppino, G., Starr, B., & Isani, S. 2001, in *SF2A-2001, Semaine de l'Astrophysique Francaise*, ed. F. Combes, D. Barret, & F. Thévenin (Paris: Obs. Paris), 605
- Davis, M., et al. 2003, *Proc. SPIE*, 4834, 161
- . 2005, in *ASP Conf. Ser. 339, Observing Dark Energy*, ed. S. C. Wolff & T. R. Lauer (San Francisco: ASP), 128
- . 2007, *ApJ*, 660, L1
- de Lucia, G., & Blaizot, J. 2007, *MNRAS*, 375, 2
- Dunlop, J. S., McLure, R. J., Kukuła, M. J., Baum, S. A., O'Dea, C. P., & Hughes, D. H. 2003, *MNRAS*, 340, 1095
- Elvis, M., et al. 1994, *ApJS*, 95, 1
- Faber, S. M., et al. 2007, *ApJ*, 665, 265
- Ferrarese, L., & Ford, H. 2005, *Space Sci. Rev.*, 116, 523
- Feulner, G., Gabasch, A., Salvato, M., Drory, N., Hopp, U., & Bender, R. 2005, *ApJ*, 633, L9
- Georgakakis, A., et al. 2006, *MNRAS*, 371, 221
- . 2007, *ApJ*, 660, L15
- . 2008, *MNRAS*, 385, 2049
- Gerke, B. F., et al. 2007, *MNRAS*, 376, 1425
- Gilli, R., Comastri, A., & Hasinger, G. 2007, *A&A*, 463, 79
- Goto, T. 2006, *MNRAS*, 369, 1765
- Graham, A. W. 2007, *MNRAS*, 379, 711
- Granato, G. L., De Zotti, G., Silva, L., Bressan, A., & Danese, L. 2004, *ApJ*, 600, 580
- Grogin, N. A., et al. 2005, *ApJ*, 627, L97
- Guainazzi, M., Matt, G., & Perola, G. C. 2005, *A&A*, 444, 119
- Hasinger, G., Miyaji, T., & Schmidt, M. 2005, *A&A*, 441, 417
- Hopkins, P. F., Cox, T. J., Keres, D., & Hernquist, L. 2008a, *ApJS*, 175, 390
- Hopkins, P. F., Hernquist, L., Cox, T. J., & Keres, D. 2008b, *ApJS*, 175, 356
- Hopkins, P. F., Hernquist, L., Martini, P., Cox, T. J., Robertson, B., Di Matteo, T., & Springel, V. 2005a, *ApJ*, 625, L71
- Hopkins, P. F., et al. 2005b, *ApJ*, 630, 705
- Hutchings, J. B., Cherniawsky, A., Cutri, R. M., & Nelson, B. O. 2006, *AJ*, 131, 680
- Ilbert, O., et al. 2006, *A&A*, 457, 841
- Juneau, S., et al. 2005, *ApJ*, 619, L135
- Kannappan, S. J., & Gawiser, E. 2007, *ApJ*, 657, L5
- Kauffmann, G., et al. 2003, *MNRAS*, 346, 1055
- La Franca, F., et al. 2005, *ApJ*, 635, 864
- Maraston, C., et al. 2006, *ApJ*, 652, 85
- Marconi, A., & Hunt, L. K. 2003, *ApJ*, 589, L21
- Marconi, A., Risaliti, G., Gilli, R., Hunt, L. K., Maiolino, R., & Salvati, M. 2004, *MNRAS*, 351, 169
- Martin, D. C., et al. 2008, *ApJS*, 173, 342
- Martini, P. 2004, in *Coevolution of Black Holes and Galaxies*, ed. L. C. Ho (Cambridge: Cambridge Univ. Press), 169
- McLure, R. J., & Dunlop, J. S. 2004, *MNRAS*, 352, 1390
- Mushotzky, R. 2004, in *Supermassive Black Holes in the Distant Universe*, ed. A. J. Barger (Dordrecht: Kluwer), 53
- Nandra, K., & Pounds, K. A. 1994, *MNRAS*, 268, 405
- Nandra, K., et al. 2005, *MNRAS*, 356, 568
- . 2007, *ApJ*, 660, L11
- Pierce, C. M., et al. 2007, *ApJ*, 660, L19
- Pozzi, F., et al. 2007, *A&A*, 468, 603
- Salim, S., et al. 2008, *ApJS*, 173, 267
- Scannapieco, E., Silk, J., & Bouwens, R. 2005, *ApJ*, 635, L13
- Schawinski, K., et al. 2007, *MNRAS*, 382, 1415
- Schmidt, M. 1968, *ApJ*, 151, 393
- Silk, J., & Rees, M. J. 1998, *A&A*, 331, L1
- Silverman, J. D., et al. 2008, *ApJ*, 675, 1025
- Somerville, R. S., Primack, J. R., & Faber, S. M. 2001, *MNRAS*, 320, 504
- Treister, E., et al. 2006, *ApJ*, 640, 603
- Treu, T., Ellis, R. S., Liao, T. X., & van Dokkum, P. G. 2005, *ApJ*, 622, L5
- Ueda, Y., Akiyama, M., Ohta, K., & Miyaji, T. 2003, *ApJ*, 598, 886
- Wild, V., Kauffmann, G., Heckman, T., Charlot, S., Lemson, G., Brinchmann, J., Reichard, T., & Pasquali, A. 2007, *MNRAS*, 381, 543
- Willmer, C. N. A., et al. 2006, *ApJ*, 647, 853
- Wilson, J. C., et al. 2003, *Proc. SPIE*, 4841, 451
- Woo, J.-H., Treu, T., Malkan, M. A., & Blandford, R. D. 2006, *ApJ*, 645, 900
- Yan, R., Newman, J. A., Faber, S. M., Konidaris, N., Koo, D., & Davis, M. 2006, *ApJ*, 648, 281
- Yang, Y., Tremonti, C. A., Zabludoff, A. I., & Zaritsky, D. 2006, *ApJ*, 646, L33